PERGAMON

International Journal of Solids and Structures 40 (2003) 219–236

INTERNATIONAL JOURNAL OF SOLIDS and STRUCTURES

www.elsevier.com/locate/ijsolstr

Fracture mechanics analysis of curved stiffened panels using BEM

P.H. Wen [a], M.H. Aliabadi [a,*], A. Young [b]

[a] *Engineering Department, Queen Mary, University of London, Mile End Road, London E1 4NS, UK*
[b] *Structural Materials Centre, DERA, Farnborough, Hants, GU14 6TD, UK*

Received 11 June 2001; received in revised form 12 August 2002

Abstract

A dual boundary element method is developed for a analysis of reinforced cracked shallow shells. Boundary integral equations are derived from the Betti's reciprocal theorem for a cracked shallow shell with transverse frames and longitudinal stiffeners. The effect of frames and stiffeners are treated as a distribution of line body forces. The radial basis function is used to transform domain integrals to boundary integrals. Stress intensity factors are evaluated from crack opening displacements. The effect of curvature on the stress intensity factors is illustrated by numerical examples. Three examples are presented to demonstrate the accuracy of this method compared with solutions obtained using the finite element method.

Keywords: Boundary element method; Stiffened shallow shells; Fracture mechanics; Stress intensity factors

1. Introduction

Enhanced quality control procedures introduced at the manufacturing stage aim to ensure aircraft are free of structural flaws. However, since the early 1950s, experience has shown that the ability to tolerate a substantial amount of damage is a requirement for modern aircraft. For transport aircraft the skin structure of a pressurized fuselage is fatigue sensitive. Therefore accurate fatigue and residual strength estimations of the critical components must be carried out to ensure safe operation. Aircraft fuselages are made of thin sheets of metal (i.e. a skin) reinforced by longitudinal and transverse stiffeners. The stiffeners can be attached to the sheet by means of fasteners, bonded to it or, alternatively, machined to form an integral panel. The longitudinal and transverse membranes are used to divide the skin into small panels, so increasing the bulkling and failing loads as well as assisting the skin in resisting bending, axial loads and hoop stress caused by pressurization of the aircraft. The stiffeners provide an alternative path for the panel load to pass around a cracked skin. If a skin crack reaches a critical length and a skin fracture begins, the

* Corresponding author. Tel.: +44-20-7882-5301; fax: +44-20-983-1007.
E-mail address: m.h.aliabadi@qmw.ac.uk (M.H. Aliabadi).

0020-7683/02/$ - see front matter
PII: S0020-7683(02)00498-5

load is transferred from the skin to the stiffeners and the fracture is arrested. Fracture mechanics provides the concepts and mathematical basis for damage tolerance design.

Configurations involving cracks in infinite or semi-infinite plates with riveted stiffeners or stringers have been studied by several authors (see, for example, Romualdi et al., 1957; Sanders, 1959; Greif and Sanders, 1965; Salgado and Aliabadi, 1998). By using Reissner's plate theory and the Fourier integral transform technique, an analytical solution for a stiffened plate containing a through-crack subjected to a uniform bending load was obtained by Yahsi and Shahid (1986). The asymptotic stress state near the crack tip terminating at the stiffener was also examined in Yahsi and Shahid (1986). More recently, attention has been paid to curved panels used in the fuselage section (see Schijve, 1995). It is generally recognized that cracks in curved shells behave differently from cracks in flat sheets. This is mainly due to the curvature which causes amplification of the crack opening displacements (CODs) in the shells compared with to the case of a crack on a plate subjected to identical membrane loading conditions. Application of the finite element method to cracked curved panels can be found in Barsoum et al. (1979) and Huang et al. (1997a,b).

The application of the boundary integral equation method to the plate bending problem was presented by Jaswon and Maiti (1968) using classical theory. For the Reissner plate model, the boundary integral equation was derived by Vander Weeën (1982) and fundamental solutions were deduced using the Hormander method. A review of the application of the boundary element method to plate bending problems can be found in the book by Aliabadi (1998). A displacement integral equation for a shear deformable shell was derived by Dirgantara and Aliabadi (1999) and the cell technique was used to treat the domain integrals. Recently Wen et al. (2002a) developed the dual reciprocity method to transform domain integrals into boundary integrals in BEM analysis for shell problems and studied reinforced shells Wen et al. (2002b). Hypersingular formulation for cracked shells was presented by Dirgantara and Aliabadi (2001). A comprehensive coverage of BEM formulations can be found in a two volume text book by Wrobel (2002) and Aliabadi (2002).

In this paper, based on the shear deformable plate theory, the dual boundary integral equations are presented for stiffened shallow shells. The couple terms are treated as body forces and the boundary values of rotations and deflection for plate bending and displacements for the two-dimensional in-plane problem are determined for a cracked panel by solving the dual integral equations. The effects of stiffeners on the reinforced shell are described; the line body forces and the distributions of these body forces are determined by the displacement connection conditions. Stress intensity factors for both bending and in-plane problems are obtained by CODs. Several examples are presented and comparisons are made with the finite element method to demonstrate the accuracy of the proposed method.

2. Boundary integral equations for a cracked shell

Consider a shallow shell, as shown in Fig. 1(a), with a quadratic middle surface given by

$$z = -\frac{1}{2}(k_{11}x_1^2 + k_{22}x_2^2) \tag{1}$$

where k_{11} and k_{22} are the principal curvatures of the shell in the x_1- and x_2-directions respectively. The equilibrium equations can be written in terms of displacements for plane stress elasticity as

$$L^{\mathrm{K}}_{\alpha\beta}u_\beta + f_\alpha = 0 \tag{2}$$

and, for plate bending,

$$L^{\mathrm{V}}_{ik}w_k + q_i = 0 \tag{3}$$

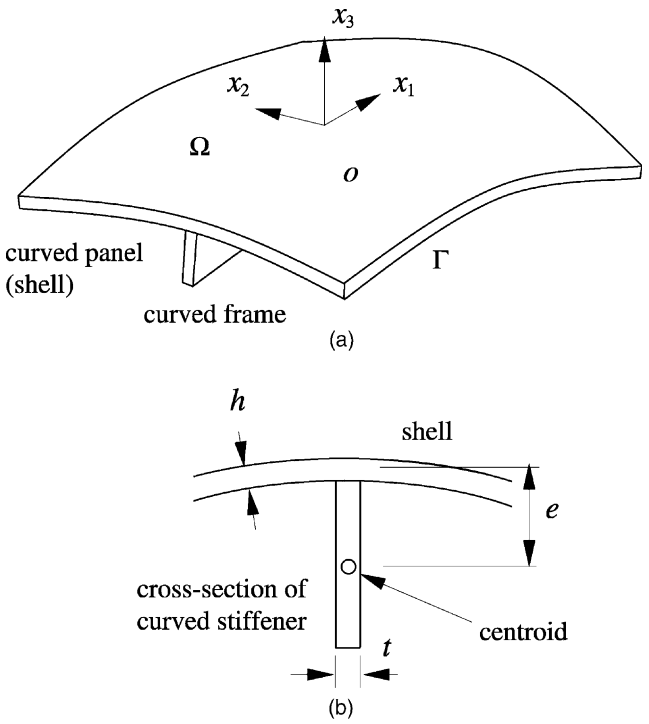

Fig. 1. Curved stiffened panel and curved stiffener.

where Greek indices vary from 1 to 2 and Roman indices vary from 1 to 3. The Navier differential operators $L^{\mathrm{K}}_{\alpha\beta}$ and L^{V}_{ik} are defined in Wen et al. (2002a). The equivalent body forces for plane stress elasticity are given as

$$f_\alpha = f^0_\alpha + B[(1-v)k_{\alpha\beta} + vk_{\phi\phi}\delta_{\alpha\beta}]w_{3,\beta} \tag{4}$$

and, for plate bending as

$$q_1 = q_2 = 0$$

$$q_3 = q^0_3 - B[(1-v)k_{\alpha\beta} + vk_{\phi\phi}\delta_{\alpha\beta}]u_{\alpha,\beta} - B(k^2_{11} + k^2_{22} + 2vk_{11}k_{22})w_3 \tag{5}$$

where u_α and w_3 are translations of displacements in x_1-, x_2- (two-dimension) and x_3-directions and w_α are rotations in the x_α-direction. The body forces applied on the shell are denoted by f^0_α and q^0_3 along the x_α- and x_3-directions respectively. The material parameter $B = Eh/(1-v^2)$ is tension stiffness, $D = Eh^3/12(1-v^2)$ is bending stiffness of the plate, h is the thickness of the plate; and E and v are the elastic constants.

By using Betti's reciprocal theorem, displacements for plane stress two-dimensional elasticity at $\mathbf{X}'$ in the domain Ω can be written as (see Wen et al., 2002a; Aliabadi, 2002)

$$\begin{aligned} u_\alpha(\mathbf{X}') = {} & \int_\Gamma U^{\mathrm{K}}_{\alpha\beta}(\mathbf{X}',\mathbf{x})t_\beta(\mathbf{x})\,\mathrm{d}\Gamma(\mathbf{x}) - B[(1-v)k_{\beta\gamma} + vk_{\phi\phi}\delta_{\beta\gamma}]\int_\Gamma U^{\mathrm{K}}_{\alpha\beta}(\mathbf{x}',\mathbf{x})n_\gamma(\mathbf{x})w_3(\mathbf{x})\,\mathrm{d}\Gamma(\mathbf{x}) \\ & - \int_\Gamma T^{\mathrm{K}}_{\alpha\beta}(\mathbf{X}',\mathbf{x})u_\beta(\mathbf{x})\,\mathrm{d}\Gamma(\mathbf{x}) + \int_\Omega U^{s}_{\alpha\beta}(\mathbf{X}',\mathbf{X})f_\beta(\mathbf{X})\,\mathrm{d}\Omega(\mathbf{X}) \end{aligned} \tag{6}$$

where $t_\alpha = N_{\alpha\beta}n_\beta$; $U^{\mathrm{K}}_{\alpha\beta}(\mathbf{x}',\mathbf{x})$ and $T^{\mathrm{K}}_{\alpha\beta}(\mathbf{x}',\mathbf{x})$ are displacement and traction fundamental solutions for the plane stress condition (Kelvin's solutions). The rotations and deflection w_i at $\mathbf{X}'$ in the domain Ω can be obtained from

$$w_i(\mathbf{X}') = \int_\Gamma U^{\mathrm{V}}_{ik}(\mathbf{X}',\mathbf{x})p_k(\mathbf{x})\,\mathrm{d}\Gamma(\mathbf{x}) - \int_\Gamma T^{\mathrm{V}}_{ik}(\mathbf{X}',\mathbf{x})w_k(\mathbf{x})\,\mathrm{d}\Gamma(\mathbf{x}) + \int_\Omega U^{\mathrm{V}}_{ik}(\mathbf{X}',\mathbf{X})q_k(\mathbf{X})\,\mathrm{d}\Omega(\mathbf{X}) \tag{7}$$

where $p_\alpha = M_{\alpha\beta}n_\beta$, $p_3 = Q_\beta n_\beta$ and U^{V}_{ij}, T^{V}_{ij} are displacement and traction fundamental solutions respectively for the plate bending problem. The boundary integral equations can be obtained by considering the limit as the domain point $\mathbf{X}'$ to a boundary point $\mathbf{x}'$. Substituting (4) and (5) into Eqs. (6) and (7), the boundary integral equation (10) for the shallow shell problem can be written as

$$\begin{aligned} &c^{\mathrm{K}}_{\alpha\beta}(\mathbf{x}')u_\beta(\mathbf{x}') + \fint_\Gamma T^{\mathrm{K}}_{\alpha\beta}(\mathbf{x}',\mathbf{x})u_\beta(\mathbf{x})\,\mathrm{d}\Gamma(\mathbf{x}) - \int_\Gamma U^{\mathrm{K}}_{\alpha\beta}(\mathbf{x}',\mathbf{x})t_\beta(\mathbf{x})\,\mathrm{d}\Gamma(\mathbf{x}) + B[(1-\nu)k_{\beta\gamma} + \nu k_{\phi\phi}\delta_{\beta\gamma}] \\ &\quad\times \int_\Gamma U^{\mathrm{K}}_{\alpha\gamma}(\mathbf{x}',\mathbf{x})n_\beta(\mathbf{x})w_3(\mathbf{x})\,\mathrm{d}\Gamma(\mathbf{x}) - B\int_\Omega U^{\mathrm{K}}_{\alpha\beta}(\mathbf{x}',\mathbf{X})[(1-\nu)k_{\beta\gamma} + \nu k_{\phi\phi}\delta_{\beta\gamma}]w_{3,\gamma}(\mathbf{X})\,\mathrm{d}\Omega(\mathbf{X}) \\ &\quad= \int_\Omega U^{\mathrm{K}}_{\alpha\beta}(\mathbf{x}',\mathbf{X})f^0_\beta(\mathbf{X})\,\mathrm{d}\Omega(\mathbf{X}) \end{aligned} \tag{8}$$

for plane stress, where $\fint$ denotes a Cauchy principal-value integral, and

$$\begin{aligned} &c^{\mathrm{V}}_{ik}(\mathbf{x}')w_k(\mathbf{x}') + \fint_\Gamma T^{\mathrm{V}}_{ik}(\mathbf{x}',\mathbf{x})w_k(\mathbf{x})\,\mathrm{d}\Gamma(\mathbf{x}) - \int_\Gamma U^{\mathrm{V}}_{ik}(\mathbf{x}',\mathbf{x})p_k(\mathbf{x})\,\mathrm{d}\Gamma(\mathbf{x}) + B[(1-\nu)k_{\alpha\beta} + \nu k_{\phi\phi}\delta_{\alpha\beta}] \\ &\quad\times \int_\Omega U^{\mathrm{V}}_{i3}(\mathbf{x}',\mathbf{X})u_{\alpha,\beta}\,\mathrm{d}\Omega - B(k_{11}^2 + k_{22}^2 + 2\nu k_{11}k_{22})\int_\Omega U^{\mathrm{V}}_{i3}(\mathbf{x}',\mathbf{X})w_3\,\mathrm{d}\Omega = \int_\Omega U^{\mathrm{V}}_{i3}(\mathbf{x}',\mathbf{X})q^0_3\,\mathrm{d}\Omega \end{aligned} \tag{9}$$

for plate bending. The free terms $c^{\mathrm{K}}_{\alpha\beta}(\mathbf{x}')$ and $c^{\mathrm{V}}_{ik}(\mathbf{x}')$ are functions of the geometry at the boundary points which can be determined by considering rigid body movements.

On one of the crack surfaces, traction boundary integral equations with hypersingularities can be written as follows (see Dirgantara and Aliabadi, 2001):

$$\begin{aligned} \frac{1}{2}t_\alpha(\mathbf{x}^+) - \frac{1}{2}t_\alpha(\mathbf{x}^-) &= n_\beta \fint_\Gamma U^{\mathrm{K}}_{\alpha\beta\gamma}(\mathbf{x}^+,\mathbf{x})t_\gamma(\mathbf{x})\,\mathrm{d}\Gamma(\mathbf{x}) - n_\beta \fint_\Gamma T^{\mathrm{K}}_{\alpha\beta\gamma}(\mathbf{x}^+,\mathbf{x})u_\gamma(\mathbf{x})\,\mathrm{d}\Gamma(\mathbf{x}) \\ &\quad - n_\beta B[(1-\nu)k_{\theta\gamma} + \nu k_{\phi\phi}\delta_{\theta\gamma}]\int_\Gamma U^{\mathrm{K}}_{\alpha\beta\gamma}(\mathbf{x}^+,\mathbf{x})n_\theta(\mathbf{x})w_3(\mathbf{x})\,\mathrm{d}\Gamma(\mathbf{x}) \\ &\quad + n_\beta B\int_\Omega U^{\mathrm{K}}_{\alpha\beta\gamma}(\mathbf{x}^+,\mathbf{X})[(1-\nu)k_{\theta\gamma} + \nu k_{\phi\phi}\delta_{\theta\gamma}]w_{3,\theta}(\mathbf{X})\,\mathrm{d}\Omega(\mathbf{X}) \\ &\quad + n_\beta \int_\Omega U^{\mathrm{K}}_{\alpha\beta\gamma}(\mathbf{x}^+,\mathbf{X})q_\gamma(\mathbf{X})\,\mathrm{d}\Omega(\mathbf{X}) \end{aligned} \tag{10}$$

for two-dimensions and

$$\begin{aligned} \frac{1}{2}p_i(\mathbf{x}^+) - \frac{1}{2}p_i(\mathbf{x}^-) &= n_\beta \fint_\Gamma U^{\mathrm{V}}_{i\beta k}(\mathbf{X}^+,\mathbf{x})p_k(\mathbf{x})\,\mathrm{d}\Gamma(\mathbf{x}) - n_\beta \fint_\Gamma T^{\mathrm{V}}_{i\beta k}(\mathbf{X}^+,\mathbf{x})w_k(\mathbf{x})\,\mathrm{d}\Gamma(\mathbf{x}) \\ &\quad - n_\beta B[(1-\nu)k_{\gamma\theta} + \nu k_{\phi\phi}\delta_{\gamma\theta}]\int_\Omega U^{\mathrm{V}}_{i\beta3}(\mathbf{x}^+,\mathbf{X})u_{\gamma,\theta}\,\mathrm{d}\Omega - n_\beta B(k_{11}^2 + k_{22}^2 + 2\nu k_{11}k_{22}) \\ &\quad \times \int_\Omega U^{\mathrm{V}}_{i\beta3}(\mathbf{x}^+,\mathbf{X})w_3\,\mathrm{d}\Omega + n_\beta \int_\Omega U^{\mathrm{V}}_{i\beta k}(\mathbf{x}^+,\mathbf{X})q^0_k\,\mathrm{d}\Omega \end{aligned} \tag{11}$$

where $\mathbf{x}^+$, $\mathbf{x}^-$ denote the collocation points on the crack's upper and lower surfaces respectively, $\fint$ denotes a Hadamard principal-value integral, $U^{\mathrm{K}}_{\alpha\beta\gamma}$, $T^{\mathrm{K}}_{\alpha\beta\gamma}$ and $U^{\mathrm{V}}_{i\beta k}$, $T^{\mathrm{V}}_{i\beta k}$ contain derivatives of fundamental solutions

(see Dirgantara and Aliabadi, 2001 for details). It can be seen that the BEM solutions for the shallow shell problem can be solved from boundary integral equations (8)–(11) by the coupling of plane stress two-dimensional elasticity and the plate bending problem. The domain integrals contain coupling terms in equivalent body forces f_α and q_3^0 in the equations. In the boundary integral equations (8)–(11), there are 12 domain integrals in the absence of body force (i.e. $f_1^0 = f_2^0 = 0$). They can be transformed to boundary integrals by using the dual reciprocity method (see Wen et al., 2002a; Dirgantara and Aliabadi, 2001; Aliabadi, 2002 for details).

Considering the properties of the fundamental solution as below:

$$U_{\alpha\beta}(\mathbf{x}'^{+},\mathbf{x}) = U_{\alpha\beta}(\mathbf{x}'^{-},\mathbf{x}), \quad U_{\alpha\beta\gamma}(\mathbf{x}'^{+},\mathbf{x}) = U_{\alpha\beta\gamma}(\mathbf{x}'^{-},\mathbf{x})$$

and

$$T_{\alpha\beta}(\mathbf{x}'^{+},\mathbf{x}) = -T_{\alpha\beta}(\mathbf{x}'^{-},\mathbf{x}), \quad T_{\alpha\beta\gamma}(\mathbf{x}'^{+},\mathbf{x}) = -T_{\alpha\beta\gamma}(\mathbf{x}'^{-},\mathbf{x})$$

If $t_\beta^+ + t_\beta^- = 0$ for two-dimensions, the boundary integral equations (1) and (8) can be rewritten as

$$\begin{aligned} &c_{\alpha\beta}^{\mathrm{K}}(\mathbf{x}')u_\beta(\mathbf{x}') + \oint_{\Gamma_0} T_{\alpha\beta}^{\mathrm{K}}(\mathbf{x}',\mathbf{x})u_\beta(\mathbf{x})\,\mathrm{d}\Gamma + \int_{C^+} T_{\alpha\beta}^{\mathrm{K}}(\mathbf{x}',\mathbf{x}^+)\,\Delta u_\beta\,\mathrm{d}\Gamma - \int_{\Gamma_0} U_{\alpha\beta}^{\mathrm{K}}(\mathbf{x}',\mathbf{x})t_\beta(\mathbf{x})\,\mathrm{d}\Gamma \\ &\quad + B[(1-\nu)k_{\beta\gamma} + \nu k_{\phi\phi}\delta_{\beta\gamma}]\left(\int_{\Gamma_0} U_{\alpha\gamma}^{\mathrm{K}}(\mathbf{x}',\mathbf{x})n_\beta(\mathbf{x})w_3\,\mathrm{d}\Gamma + \int_{C^+} U_{\alpha\gamma}^{\mathrm{K}}(\mathbf{x}',\mathbf{x})n_\beta(\mathbf{x})\,\Delta w_3(\mathbf{x})\,\mathrm{d}\Gamma\right) \\ &\quad - B\int_\Omega U_{\alpha\beta}^{\mathrm{K}}(\mathbf{x}',\mathbf{X})[(1-\nu)k_{\beta\gamma} + \nu k_{\phi\phi}\delta_{\beta\gamma}]w_{3,\gamma}(\mathbf{X})\,\mathrm{d}\Omega = \int_\Omega U_{\alpha\beta}^{\mathrm{K}}(\mathbf{x}',\mathbf{X})f_\beta^0\,\mathrm{d}\Omega \end{aligned} \tag{12}$$

for displacements and

$$\begin{aligned} \frac{1}{2}t_\alpha(\mathbf{x}^+) - \frac{1}{2}t_\alpha(\mathbf{x}^-) &= n_\beta \oint_{\Gamma_0} U_{\alpha\beta\gamma}^{\mathrm{K}}(\mathbf{x}^+,\mathbf{x})t_\gamma(\mathbf{x})\,\mathrm{d}\Gamma - n_\beta(\mathbf{x}'^{+})\int_{\Gamma_0} T_{\alpha\beta\gamma}^{\mathrm{K}}(\mathbf{x}'^{+},\mathbf{x})u_\gamma(\mathbf{x})\,\mathrm{d}\Gamma \\ &\quad - n_\beta(\mathbf{x}'^{+})\oint_{C^+} T_{\alpha\beta\gamma}^{\mathrm{K}}(\mathbf{x}'^{+},\mathbf{x}^+)\,\Delta u_\gamma\,\mathrm{d}\Gamma - n_\beta B[(1-\nu)k_{\theta\gamma} + \nu k_{\phi\phi}\delta_{\theta\gamma}] \\ &\quad \times \left(\int_{\Gamma_0} U_{\alpha\beta\gamma}^{\mathrm{K}}(\mathbf{x}^+,\mathbf{x})n_\theta(\mathbf{x})w_3\,\mathrm{d}\Gamma + \int_{C^+} U_{\alpha\beta\gamma}^{\mathrm{K}}(\mathbf{x}^+,\mathbf{x})n_\theta(\mathbf{x})\,\Delta w_3\,\mathrm{d}\Gamma\right) \\ &\quad + n_\beta B\int_\Omega U_{\alpha\beta\gamma}^{\mathrm{K}}(\mathbf{x}^+,\mathbf{X})[(1-\nu)k_{\theta\gamma} + \nu k_{\phi\phi}\delta_{\theta\gamma}]w_{3,\theta}(\mathbf{X})\,\mathrm{d}\Omega + n_\beta\int_\Omega U_{\alpha\beta\gamma}^{\mathrm{K}}(\mathbf{x}^+,\mathbf{X})q_\gamma^0\,\mathrm{d}\Omega \end{aligned} \tag{13}$$

for tractions. Similarly if $p_i^+ + p_i^- = 0$ for bending, the boundary integral equations (2) and (9) can be rewritten as

$$\begin{aligned} &c_{ik}^{\mathrm{V}}(\mathbf{x}')w_k(\mathbf{x}') + \oint_{\Gamma_0} T_{ik}^{\mathrm{V}}(\mathbf{x}',\mathbf{x})w_k(\mathbf{x})\,\mathrm{d}\Gamma + \int_{C^+} T_{ik}^{\mathrm{V}}(\mathbf{x}',\mathbf{x}^+)\,\Delta w_k\,\mathrm{d}\Gamma - \int_{\Gamma_0} U_{ik}^{\mathrm{V}}(\mathbf{x}',\mathbf{x})p_k(\mathbf{x})\,\mathrm{d}\Gamma(\mathbf{x}) \\ &\quad + B[(1-\nu)k_{\alpha\beta} + \nu k_{\phi\phi}\delta_{\alpha\beta}]\int_\Omega U_{i3}^{\mathrm{V}}(\mathbf{x}',\mathbf{X})u_{\alpha,\beta}\,\mathrm{d}\Omega - B(k_{11}^2 + k_{22}^2 + 2\nu k_{11}k_{22})\int_\Omega U_{i3}^{\mathrm{V}}(\mathbf{x}',\mathbf{X})w_3\,\mathrm{d}\Omega \\ &\quad = \int_\Omega U_{ik}^{\mathrm{V}}(\mathbf{x}',\mathbf{X})q_k^0\,\mathrm{d}\Omega \end{aligned} \tag{14}$$

for rotations and deflection, and

$$\frac{1}{2}p_i(\mathbf{x}^+) - \frac{1}{2}p_i(\mathbf{x}^-) = n_\beta \oint_{\Gamma_0} U^{\mathrm{V}}_{i\beta k}(\mathbf{X}^+, \mathbf{x}) p_k(\mathbf{x})\,\mathrm{d}\Gamma - n_\beta \int_{\Gamma_0} T^{\mathrm{V}}_{i\beta k}(\mathbf{X}^+, \mathbf{x}) w_k(\mathbf{x})\,\mathrm{d}\Gamma$$
$$- n_\beta(\mathbf{x}'^+) \oint_{C^+} T^{\mathrm{V}}_{i\beta k}(\mathbf{x}'^+, \mathbf{x}^+)\,\Delta w_k\,\mathrm{d}\Gamma - n_\beta B[(1-\nu)k_{\gamma\theta} + \nu k_{\phi\phi}\delta_{\gamma\theta}] \int_\Omega U^{\mathrm{V}}_{i\beta 3}(\mathbf{x}^+, \mathbf{X}) u_{\gamma,\theta}\,\mathrm{d}\Omega$$
$$- n_\beta B(k_{11}^2 + k_{22}^2 + 2\nu k_{11}k_{22}) \int_\Omega U^{\mathrm{V}}_{i\beta 3}(\mathbf{x}^+, \mathbf{X}) w_3\,\mathrm{d}\Omega + n_\beta \int_\Omega U^{\mathrm{V}}_{i\beta k}(\mathbf{x}^+, \mathbf{X}) q^0_k\,\mathrm{d}\Omega \qquad (15)$$

for tractions, where $\Gamma_0 = \Gamma - C^+ - C^-$ (boundaries excluding crack surfaces), C^+ and C^- represent upper and lower crack surfaces and Δu_β and Δw_k are discontinuities of displacements and defined as $\Delta u_\beta = u^+_\beta - u^-_\beta$ and $\Delta w_k = w^+_k - w^-_k$. In this case, the unknowns can be reduced to the displacements or traction on the boundary Γ_0 and discontinuity of displacement on the crack surface C. Applying the displacement integral equation on the boundary Γ_0 and the traction equation on the crack surface C^+ gives a linear system to determine all unknowns including discontinuity displacements on the crack surface Δu_β and Δw_k.

3. Numerical implementation for stiffened cracked shells

Considering a straight beam parallel to the x_1-axis and ignoring the torsional effect of a curved beam, there are only two distributions of interaction forces $f(x_1)$ and $q(x_1)$ at the top of the beam along the x_1-axis as shown in Figs. 1(b) and 2. If there is only a uniform pressure load q_0 acting on the shell, the body forces in Eqs. (4) and (5) can be written as

$$\begin{aligned} f_1(x_1, x_2) &= -f(x_1)\delta(x_2 - x_2^0) \\ f_2(x_1, x_2) &= 0 \\ q_3(x_1, x_2) &= q_3^0 - q(x)\delta(x_2 - d) \end{aligned} \qquad (16)$$

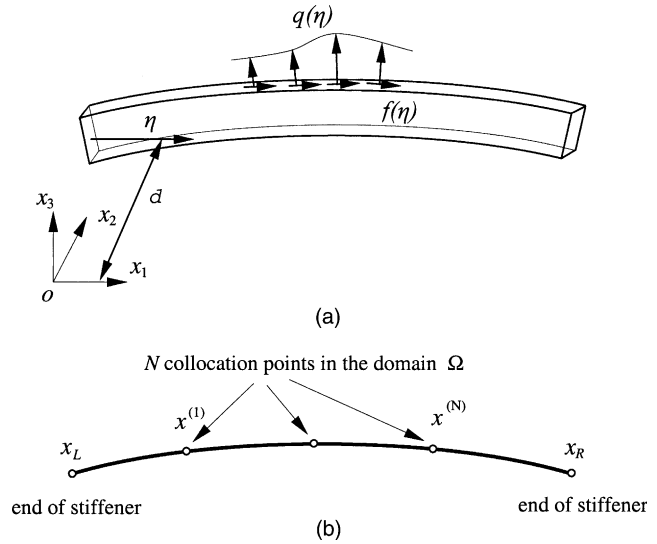

Fig. 2. Interaction forces and nodal distribution on the curved stiffener.

where $\delta(x)$ is the Dirac delta function, x denotes the local coordinate on the beam along the x_1-axis and d denotes the distance between the beam and x_1-axis. The interaction forces' nodal values can be expressed in terms of nodal values of deflection and displacement as (see Appendix A)

$$\mathbf{q} = \mathbf{Q}^{-1}\mathbf{R}\mathbf{w} - \mathbf{Q}^{-1}\mathbf{P}\mathbf{u} \tag{17}$$

and

$$\mathbf{f} = \mathbf{E}^{-1}[\mathbf{Q}'\mathbf{Q}^{-1}\mathbf{R} + \mathbf{R}']\mathbf{w} + \mathbf{E}^{-1}[\mathbf{P}' - \mathbf{Q}'\mathbf{Q}^{-1}\mathbf{P}]\mathbf{u} \tag{18}$$

Using quadratic elements, the boundary integral equation (8) can be written in a discretized form as

$$\begin{aligned} &c^{\mathrm{K}}_{\alpha\beta}(\mathbf{x}')u_\beta(\mathbf{x}') + \sum_{n=1}^{L_0}\sum_{l=1}^{3} u^l_\beta \int_{-1}^{1} T^{\mathrm{K}}_{\alpha\beta}[\mathbf{x}', \mathbf{x}(\xi)]N_l(\xi)J^n(\xi)\,\mathrm{d}\xi - \sum_{n=1}^{N_0}\sum_{l=1}^{3} t^l_\beta \int_{-1}^{1} U^{\mathrm{K}}_{\alpha\beta}[\mathbf{x}', \mathbf{x}(\xi)]N_l(\xi)J^n(\xi)\,\mathrm{d}\xi \\ &\quad - B[(1-v)k_{\beta\gamma} + vk_{\phi\phi}\delta_{\beta\gamma}]\sum_{n=1}^{N_0}\sum_{l=1}^{3} w^l_3 \int_{-1}^{1} U^{\mathrm{K}}_{\alpha\beta}[\mathbf{x}', \mathbf{x}(\xi)]N_l(\xi)J^n(\xi)n_\gamma(\mathbf{x})\,\mathrm{d}\xi - B(k_{11} + vk_{22})I_{\alpha 4} \\ &\quad - B(k_{22} + vk_{11})I_{\alpha 5} = -\int_{x_{\mathrm{L}}}^{x_{\mathrm{R}}} U^{\mathrm{K}}_{\alpha 1}(\mathbf{x}', x_1)f(x_1)\,\mathrm{d}x_1 \end{aligned} \tag{19}$$

where u^l_β, t^l_β and w^l_3 present the boundary values at each node, N_l and J^n are shape functions and Jacobian for each element, N_0 is the total number of elements and $I_{\alpha 4}$ and $I_{\alpha 5}$ are domain integrals, x_{L}, x_{R} are the two end coordinates of a curved beam. Similarly, Eq. (9) becomes

$$\begin{aligned} &c^{\mathrm{V}}_{ik}(\mathbf{x}')w_k(\mathbf{x}') + \sum_{n=1}^{N_0}\sum_{l=1}^{3} w^l_k \int_{-1}^{1} T^{\mathrm{V}}_{ik}[\mathbf{x}', \mathbf{x}(\xi)]N_l(\xi)J^n(\xi)\,\mathrm{d}\xi - \sum_{n=1}^{N_0}\sum_{l=1}^{3} p^l_k \int_{-1}^{1} U^{\mathrm{V}}_{ik}[\mathbf{x}', \mathbf{x}(\xi)]N_l(\xi)J^n(\xi)\,\mathrm{d}\xi \\ &\quad + B(k_{11} + vk_{22})I_{i2} + B(k_{22} + vk_{11})I_{i3} + B(k^2_{11} + k^2_{22} + 2vk_{11}k_{22})I_{i1} - I_{i6} = -\int_{x_{\mathrm{L}}}^{x_{\mathrm{R}}} U^{\mathrm{V}}_{i3}(\mathbf{x}', x_1)q(x_1)\,\mathrm{d}x_1 \end{aligned} \tag{20}$$

Using quadratic elements, the traction boundary integral equations (10) and (11) can be written in a discretized form as

$$\begin{aligned} &\frac{1}{2}[t_\alpha(\mathbf{x}^+) - t_\alpha(\mathbf{x}^-)] + n_\beta \sum_{n=1}^{N_0}\sum_{l=1}^{3} u^l_\gamma \int_{-1}^{1} T^{\mathrm{K}}_{\alpha\beta\gamma}[\mathbf{x}', \mathbf{x}(\xi)]N_l(\xi)J^n(\xi)\,\mathrm{d}\xi \\ &\quad - n_\beta \sum_{n=1}^{N_0}\sum_{l=1}^{3} t^l_\gamma \int_{-1}^{1} U^{\mathrm{K}}_{\alpha\beta\gamma}[\mathbf{x}', \mathbf{x}(\xi)]N_l(\xi)J^n(\xi)\,\mathrm{d}\xi - n_\beta B[(1-v)k_{\theta\gamma} + vk_{\phi\phi}\delta_{\theta\gamma}]\sum_{n=1}^{N_0}\sum_{l=1}^{3} w^l_3 \\ &\quad \times \int_{-1}^{1} U^{\mathrm{K}}_{\alpha\beta\gamma}[\mathbf{x}', \mathbf{x}(\xi)]N_l(\xi)J^n(\xi)n_\theta(\mathbf{x})\,\mathrm{d}\xi - B(k_{11} + vk_{22})I_{\alpha 10} - B(k_{22} + vk_{11})I_{\alpha 11} \\ &\quad = -n_\beta \int_{x_{\mathrm{L}}}^{x_{\mathrm{R}}} U^{s}_{\alpha\beta 1}(\mathbf{x}', x_1)f(x_1)\,\mathrm{d}x_1 \end{aligned} \tag{21}$$

and for plate bending

$$\begin{aligned}&\frac{1}{2}[p_i(\mathbf{x}^+)-p_i(\mathbf{x}^-)]+n_\beta\sum_{n=1}^{N_0}\sum_{l=1}^{3}w_k^l\int_{-1}^{1}T^{\mathrm{V}}_{i\beta k}[\mathbf{x}',\mathbf{x}(\xi)]N_l(\xi)J^n(\xi)\,\mathrm{d}\xi\\&\quad-n_\beta\sum_{n=1}^{N_0}\sum_{l=1}^{3}p_k^l\int_{-1}^{1}U^{\mathrm{V}}_{i\beta k}[\mathbf{x}',\mathbf{x}(\xi)]N_l(\xi)J^n(\xi)\,\mathrm{d}\xi+B(k_{11}+\nu k_{22})I_{i8}+B(k_{22}+\nu k_{11})I_{i9}\\&\quad+B(k_{11}^2+k_{22}^2+2\nu k_{11}k_{22})I_{i7}-I_{i12}=-n_\beta\int_{x_{\mathrm{L}}}^{x_{\mathrm{R}}}U^{\mathrm{V}}_{i\beta3}(\mathbf{x}',x_1)q(x_1)\,\mathrm{d}x_1\end{aligned}\tag{22}$$

where domain integrals

$$\begin{aligned}&I_{i1}=\int_\Omega U^{\mathrm{V}}_{i3}w_3\,\mathrm{d}\Omega,\quad I_{i2}=\int_\Omega U^{\mathrm{V}}_{i3}\frac{\partial u_1}{\partial x_1}\,\mathrm{d}\Omega,\quad I_{i3}=\int_\Omega U^{\mathrm{V}}_{i3}\frac{\partial u_2}{\partial x_2}\mathrm{d}\Omega,\\&I_{\alpha4}=\int_\Omega U^{\mathrm{K}}_{\alpha1}\frac{\partial w_3}{\partial x_1}\mathrm{d}\Omega,\quad I_{\alpha5}=\int_\Omega U^{\mathrm{K}}_{\alpha2}\frac{\partial w_3}{\partial x_2}\mathrm{d}\Omega,\quad I_{i6}=\int_\Omega U^{\mathrm{V}}_{i3}q_3\,\mathrm{d}\Omega\end{aligned}\tag{23}$$

$$\begin{aligned}&I_{i7}=n_\beta\int_\Omega U^{\mathrm{V}}_{i\beta3}w_3\,\mathrm{d}\Omega,\quad I_{i8}=n_\beta\int_\Omega U^{\mathrm{V}}_{i\beta3}\frac{\partial u_1}{\partial x_1}\mathrm{d}\Omega,\quad I_{i9}=n_\beta\int_\Omega U^{\mathrm{V}}_{i\beta3}\frac{\partial u_2}{\partial x_2}\mathrm{d}\Omega,\\&I_{\alpha10}=n_\beta\int_\Omega U^{\mathrm{K}}_{\alpha\beta1}\frac{\partial w_3}{\partial x_1}\mathrm{d}\Omega,\quad I_{\alpha11}=n_\beta\int_\Omega U^{\mathrm{K}}_{\alpha\beta2}\frac{\partial w_3}{\partial x_2}\mathrm{d}\Omega,\quad I_{i12}=n_\beta\int_\Omega U^{\mathrm{V}}_{i\beta3}q_3^0\,\mathrm{d}\Omega\end{aligned}\tag{24}$$

can be transformed to boundary integrals by applying the dual reciprocity method using a radial bases function.

Portela et al. (1992) and Mi and Aliabadi (1992) proposed the use of the dual boundary element method for two-dimensional and three-dimensional problems respectively. A similar technique can be used for cracked shell problems (see Dirgantara and Aliabadi, 2001). The strategy used for modelling stiffened panels can be summarized as follows:

1. Displacement equations (8) and (9) are applied for collocation on non-cracked boundaries and one of the crack surface.
2. Traction equations (10) and (11) are applied for collocation on the other crack surfaces.
3. The interaction between stiffeners and shell is represented by body forces in Eqs. (13) and (14).

After the collocation point passes through all the collocation nodes on the boundary Γ and on the selected points in the domain as shown in Fig. 3, Eqs. (17)–(20) results in the following linear system of equations:

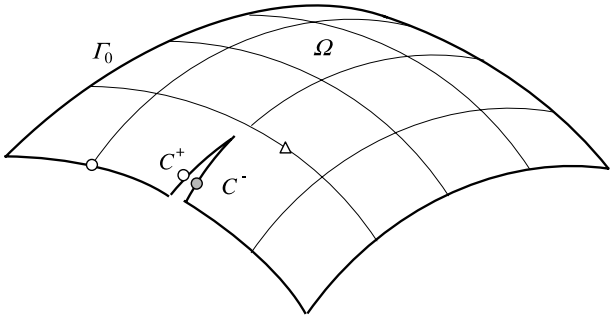

Fig. 3. Strategy of dual element method: (△) domain points (Eqs. (6) and (7)), (○) boundary points (Eqs. (8) and (9)) and (●) one of the crack surfaces (Eqs. (10) and (11)).

$$\begin{Bmatrix} \mathbf{H}^{\mathrm{K}} & \mathbf{H}^{w} \\ \mathbf{H}^{u} & \mathbf{H}^{\mathrm{K}} \end{Bmatrix} \begin{Bmatrix} \mathbf{u} \\ \mathbf{w} \end{Bmatrix} - \begin{Bmatrix} \mathbf{G}^{\mathrm{K}}\mathbf{t} \\ \mathbf{G}^{\mathrm{V}}\mathbf{p} \end{Bmatrix} = \begin{Bmatrix} \mathbf{F}^{\mathrm{K}} & \mathbf{F}^{w} \\ \mathbf{F}^{u} & \mathbf{F}^{\mathrm{V}} \end{Bmatrix} \begin{Bmatrix} \mathbf{u} \\ \mathbf{w} \end{Bmatrix} \begin{Bmatrix} \mathbf{0} \\ \mathbf{b} \end{Bmatrix} \tag{25}$$

where $\mathbf{H}^{\mathrm{K}}$, $\mathbf{G}^{\mathrm{K}}$, $\mathbf{H}^{\mathrm{V}}$ and $\mathbf{G}^{\mathrm{V}}$ are boundary element influence matrices for plane stress elasticity and the plate bending problem respectively, $\mathbf{H}^{w}$, $\mathbf{H}^{u}$ are coupling matrices caused by the shell curvatures k_{11}, k_{22} and the interaction between the beam and the shell and $\mathbf{b}$ denotes domain integrals for shear load, the last term in the above equation is from the linear integrals caused by interactions between stiffeners and shell. Considering the boundary conditions on Γ, the unknown boundary values for displacements or tractions and the displacement and deflection on the stiffener $x_2 = d$ are obtained by solving the system of equations (21).

An altenative strategy is to apply the displacement equations (8) and (9) on non-cracked boundary and traction equations (10) and (11) on one of the crack surfaces. The unknows on the crack surface are the discontinuities of displacement δu_α and δw_k which can be used to evaluate stress intensity factors.

4. Stress intensity factors evaluation

A set of special shape functions can be used to model the displacement field $\sqrt{r}$ behaviour near the crack tip (Aliabadi and Rooke, 1991). Suppose the shape function is in the form

$$N_i = a_0^i + a_1^i\sqrt{1+\eta} + a_2^i(1+\eta)$$

the shape functions for crack tip elements with the crack tip located at $\eta = -1$ are

$$\begin{aligned} N_1 &= \frac{3}{2}\frac{(3-\sqrt{15})\eta + 2\sqrt{1+\eta} - 2}{\sqrt{15}+\sqrt{3}-6} \\ N_2 &= \frac{3(3-\sqrt{15})\eta - 12\sqrt{1+\eta} + 2(\sqrt{15}+\sqrt{3})}{2(\sqrt{15}+\sqrt{3}-6)} \\ N_3 &= \frac{3}{2}\frac{(\sqrt{3}-3)\eta + 2\sqrt{1+\eta} - 2}{\sqrt{15}+\sqrt{3}-6} \end{aligned} \tag{26}$$

and for the crack tip element with the crack tip at $\eta = +1$ are

$$N_i = a_0^i + a_1^i\sqrt{1+\eta} + a_2^i(1+\eta)$$

The shape functions for the crack tip elements with the crack tip located at $\eta = -1$ are

$$\begin{aligned} N_1 &= \frac{3}{2}\frac{(\sqrt{3}-3)\eta + 2\sqrt{1-\eta} - 2}{\sqrt{15}+\sqrt{3}-6} \\ N_2 &= \frac{3(3-\sqrt{15})\eta - 12\sqrt{1-\eta} + 2(\sqrt{15}+\sqrt{3})}{2(\sqrt{15}+\sqrt{3}-6)} \\ N_3 &= \frac{3}{2}\frac{(3-\sqrt{15})\eta + 2\sqrt{1-\eta} - 2}{\sqrt{15}+\sqrt{3}-6} \end{aligned} \tag{27}$$

The accuracy of the results can be improved by using two points interpolation used in this paper with special elements near the crack tips (see Dirgantara and Aliabadi, 2001; Aliabadi, 2002). Stress intensity factors for the in-plane problem and bending problem are obtained from the following equations. The relationships between discontinuity displacements and stress intensity factors can be written as

$$\begin{aligned}
\Delta u_1 &= u_1^+ - u_1^- = \frac{8\sqrt{r}}{E\sqrt{2\pi}} K_1^m \\
\Delta u_2 &= u_2^+ - u_2^- = \frac{8\sqrt{r}}{E\sqrt{2\pi}} K_2^m \\
\Delta w_1 &= w_1^+ - w_1^- = \frac{48\sqrt{2r}}{Eh^3} K_2^b \\
\Delta w_2 &= w_2^+ - w_2^- = \frac{48\sqrt{2r}}{Eh^3} K_1^b \\
\Delta w_3 &= w_3^+ - w_3^- = \frac{24(1+\nu)\sqrt{2r}}{5Eh} K_3^b
\end{aligned} \tag{28}$$

where K_α^m, K_i^b ($\alpha = 1, 2$, $i = 1, 2, 3$) are membrane stress intensity factors and bending stress intensity factors respectively. Stress intensity factors are evaluated either by one point near the crack tip or by the two points interpolation formula. The final stress intensity factors along the thickness of the shell are given as

$$\begin{aligned}
K_{\mathrm{I}}(x_3) &= K_1^m + \frac{12x_3}{h^3} K_1^b \\
K_{\mathrm{II}}(x_3) &= K_2^m + \frac{12x_3}{h^3} K_2^b \\
K_{\mathrm{III}}(x_3) &= \frac{3}{2h}\left[1 - \left(\frac{2x_3}{h}\right)^2\right] K_3^b
\end{aligned} \tag{29}$$

5. Numerical examples

In this section three examples involving stiffened cylindrical shells containing either one or two cracks are presented.

Example 1 (*Cylindrical shell with double stiffeners and a central crack*)**.** Consider a simply supported stiffened cylindrical shell (see Fig. 4) subjected to a uniform pressure load q_0. The geometric parameters for the shell are chosen as: thickness $h = 0.05a$, crack length $c = 0.2a$, distance between stiffener $d = 0.4a$ and curvatures $k = k_{11} = 0.1/a$, $k_{22} = 0$. The Poisson ratio $\nu = 0.3$ and elasticity modulus is E. The stiffeners have rectangular cross-section with area $A = 0.05 \times 0.4a^2$. The parameters of the stiffeners are taken to be the same as the cylindrical shell. The components of displacement and deflection are defined on the boundary as

$$\begin{aligned}
&u_2 = w_3 = 0 \quad \text{at } x = \pm a \\
&t_1 = p_1 = p_2 = 0 \quad \text{at } x = \pm a \\
&u_2 = w_3 = 0 \quad \text{at } y = \pm a \\
&t_1 = p_1 = p_2 = 0 \quad \text{at } y = \pm a
\end{aligned}$$

and

$$u_1 = 0 \quad \text{at } x = \pm a \text{ and } y = 0.$$

A BEM mesh with 40 quadratic boundary elements and 64 DRM domain points are used and the number of nodes for each beam $N = 3$ is as shown in Fig. 4. The results obtained for displacements,

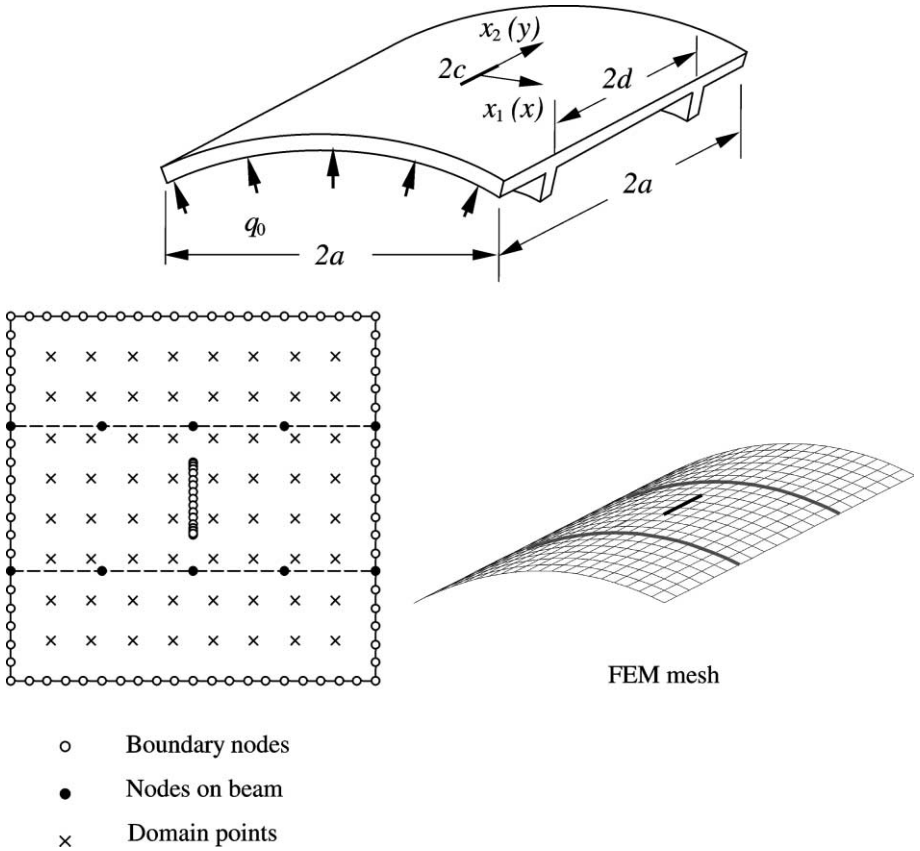

Fig. 4. A cracked cylindrical shell with two transverse frames under pressure load.

deflections and rotations along the y-axis of the cylinder are shown in Fig. 5(a)–(e). The finite element results using a software package (SAP90), with 16×16 four-node linear elements, shown in Fig. 5, are also plotted in the figures for comparison. Due to symmetry of the structure, only a quarter of the shell is considered for the finite element analysis. Normalized stress intensity factors $K_1^b/q_0\sqrt{\pi c} = 0.014$ and $K_1^m/q_0\sqrt{\pi c} = 16.09$. The maximum value of the stress intensity factor, from Eq. (27), $K_1^{\max}/q_0\sqrt{\pi c} = 49.7$. Good agreement is achieved for displacements u_1, u_2 and deflection w_3 with the finite element method. Because the classical plate theory (thin plate) is used in the finite element method, the difference between FEM and BEM results for rotation w_1 is quite large.

Example 2 (*Simply supported cylindrical shell with a central crack, two longitudinal stiffeners and two transverse frames*)**.** Consider a cylindrical shell with two longitudinal stiffeners, two transverse frames and a central crack of length $2c$ subjected to uniform pressure load q_0 (see Fig. 6). The materials are the same for the shell and stiffeners and the constants are chosen as $E = 73\,000$ MPa, $v = 0.33$. The cross-sectional areas of each frame and stiffener are taken as $A = 0.0175a^2$ and the moment of inertia to the mid-plane of the shell $I_s = 1.0193 \times 10^{-4}a^4$ and parameter $e = 0.1214a$. The prescribed boundary conditions are

$$w_3 = 0 \quad \text{at } x_1 = \pm a \quad \text{and} \quad x_2 = \pm a$$
$$t_1 = t_2 = p_1 = p_2 = 0 \quad \text{at } x_1 = \pm a, \quad \text{and} \quad x_2 = \pm a$$

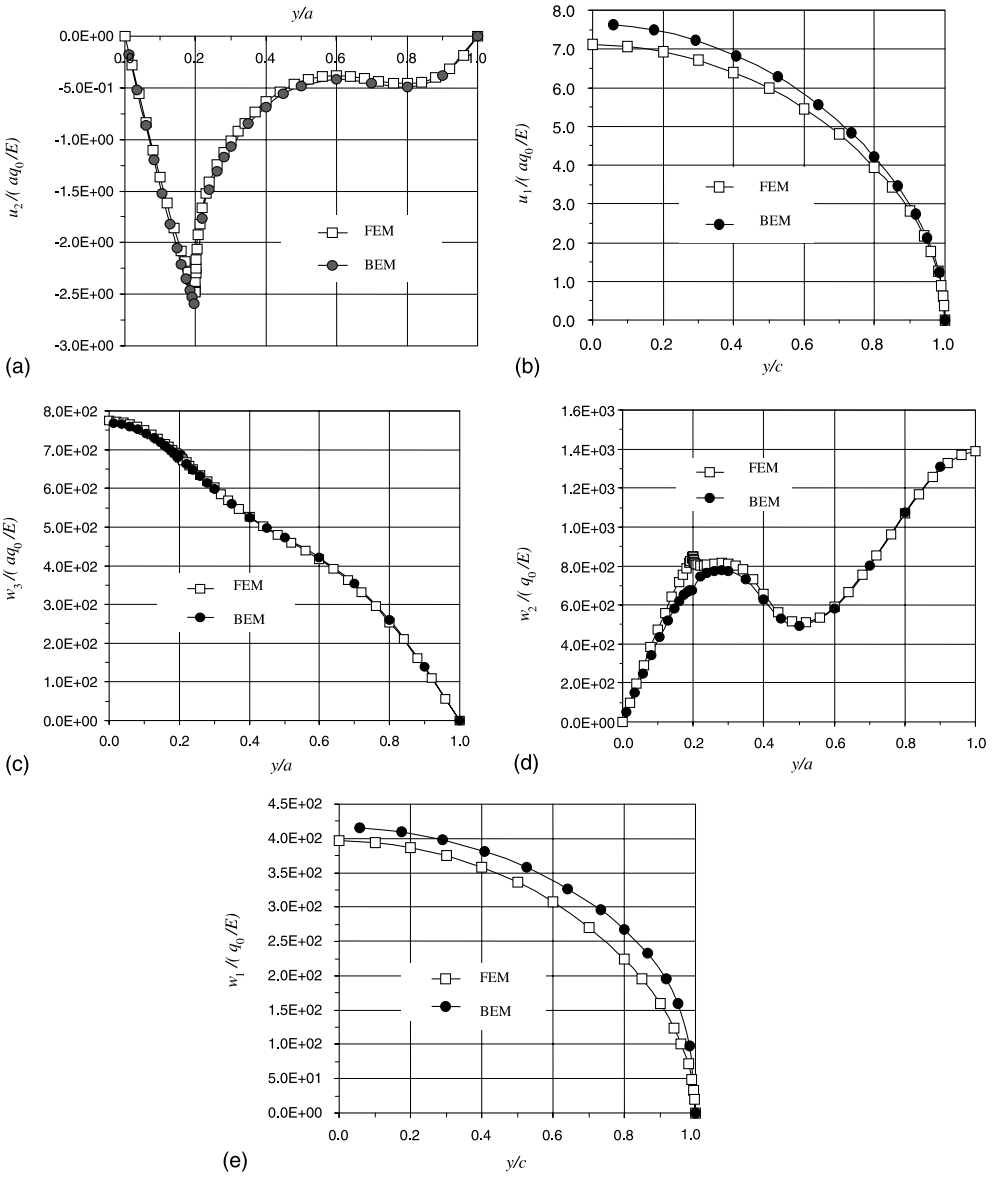

Fig. 5. Comparison of BEM and FEM results: (a, b) displacements, (c) deflection and (d, e) rotations of stiffened cylindrical shell.

$$u_1 = 0 \quad \text{at } x_1 = \pm a \quad \text{and} \quad x_2 = 0$$
$$t_2 = p_1 = p_2 = p_3 = 0 \quad \text{at } x_1 = \pm a \quad \text{and} \quad x_2 = 0$$

$$u_2 = 0 \quad \text{at } x_2 = \pm a \quad \text{and} \quad x_1 = 0$$
$$t_1 = p_1 = p_2 = p_3 = 0 \quad \text{at } x_2 = \pm a \quad \text{and} \quad x_1 = 0$$

The same BEM mesh and distribution of DRM domain points as in Example 1 are used with five nodes on the beam (i.e. $N = 5$). Because of the symmetry of load and configuration, there are only two stress

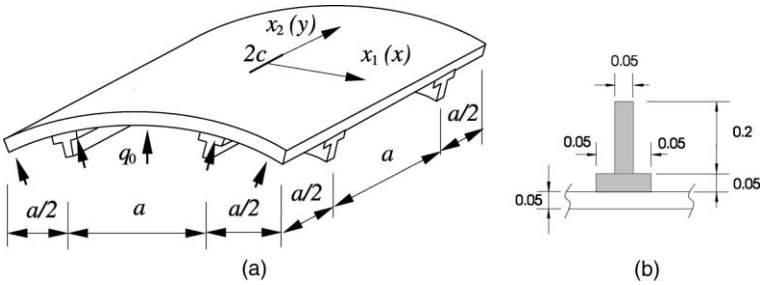

Fig. 6. Central cracked cylindrical shell with two stiffeners and two frames under internal pressure.

intensity factors at the crack tips K_{I}^{b} and K_{I}^{m}. The numerical results of the stress intensity factors due to uniform pressure are plotted against the half-length of crack c and the dimensionless factor ak_{11} ($k_{22} = 0$) in Fig. 7(a) and (b). The normalized stress intensity factors tend to decrease as the curvature tends to zero (i.e. flat plate problem). It can be seen that the moment stress intensity factor K_{I}^{b} and membrane stress intensity factor K_{I}^{m} decrease as c/a tends to 0.5 where the frame is located. The maximum stress intensity factors $K_{\mathrm{I}}^{\max}$ which occur on the top surface of the shell are shown in Fig. 7(c).

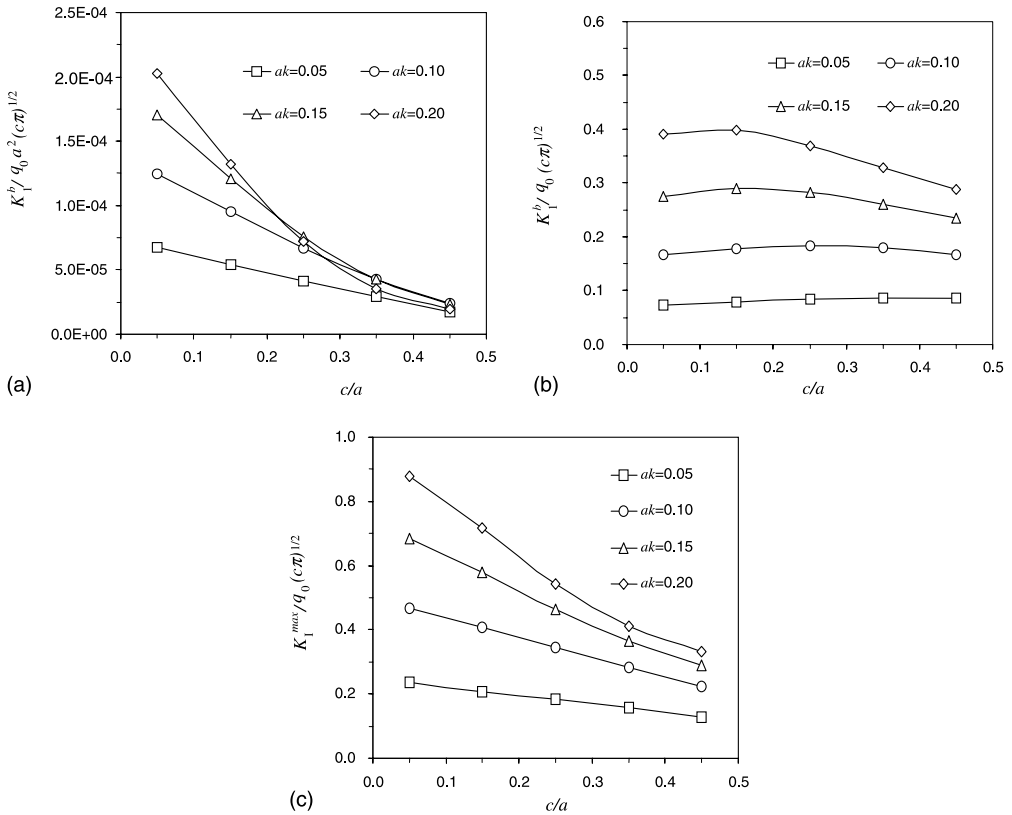

Fig. 7. Normalized stress intensity factors: (a) bending, (b) membrane and (c) maximum values ($k = k_{11}$ and denotes the coefficient of curvature).

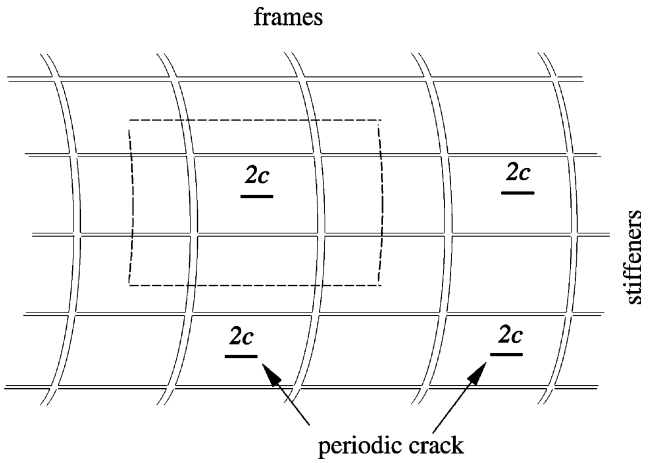

Fig. 8. Cracked fuselage panel.

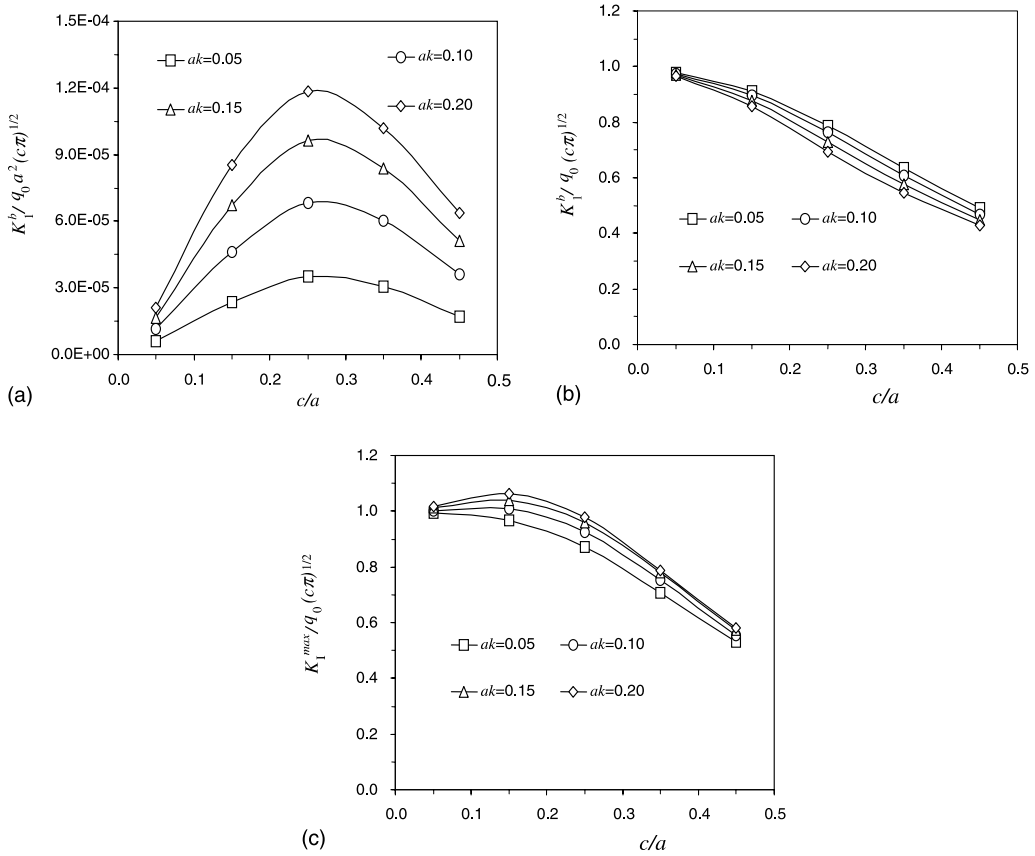

Fig. 9. Normalized stress intensity factors for cracked fuselage panel: (a) bending, (b) membrane and (c) maximum values.

Example 3 (*A cylinder with periodic stiffeners and frames and cracks subjected to internal pressure*)**.** Consider a long cylinder (fuselage) stiffened with longitudinal stiffeners and frames containing periodic cracks as shown in Fig. 8. Owing to the symmetry of the structure, only a small part of the fuselage which is cut along the dashed lines in Fig. 7 is analysed with the following boundary conditions:

$$u_1 = w_1 = 0 \quad \text{at } x_1 = \pm a$$
$$t_2 = p_2 = p_3 = 0 \quad \text{at } x_1 = \pm a$$

$$u_2 = w_2 = 0 \quad \text{at } x_2 = \pm a$$
$$t_1 = p_1 = p_3 = 0 \quad \text{at } x_2 = \pm a$$

The material parameters of the shell, frames and stiffeners and the geometrical dimensions are the same as in Example 2. As in Example 2, there are only two stress intensity factors at the crack tips K_1^b and K_1^m (because of the symmetry of load and structure). Normalized stress intensity factors for the bending problem and for the plane stress problem are plotted against the half length of crack c and dimensionless factor ak in Fig. 9(a) and (b). The normalized stress intensity factors of bending K_1^b are very small and K_1^m are close to 1 for small curvatures as the membrane forces are significant in this case. Also it can be seen that the moment stress intensity factor K_1^b and membrane stress intensity factor K_1^m decrease as c/a tends to 0.5. The maximum values of stress intensity factors K_I are shown in Fig. 9(c).

6. Conclusions

A new boundary element formulation for analysis of curved stiffened cracked panels was presented in this paper. The coupled boundary element formulation was achieved by using the two-dimensional plane stress elasticity and shear deformable plate. The interaction forces were determined in terms of the deflection of the curved beam. The dual boundary element method for analysis of stiffened cracked shells was developed. The domain integrals in displacement and traction boundary integral equations were transformed to boundary integrals by the dual reciprocity method. By solving integral equations, displacements for the in-plane problem and deflection and rotations for the plate can be obtained numerically. Stress intensity factors: two for in-plane and three for bending problems, were evaluated from two points discontinuity displacements near the crack tips. The numerical examples indicate that the boundary element method is an efficient and accurate method of analysis for cracks in stiffened shell structures.

Acknowledgements

This work has been carried out with the support of the Ministry of Defence, Defence Evaluation and Research Agency, Farnborough, UK.

Appendix A. Interaction forces between shell and stiffeners

For convenience the following analysis assume that $x = x_1$ and $y = x_2$. Consider a stiffened shell as shown in Fig. 1 with a stiffener at $y = 0$. The differential equations can be deduced from the fundamental equations for the shell problem in Cartesian coordinates as follows (Chinh, 1997; Wen et al., 2002b):

$$\frac{d^2 u_0}{dx^2} + k\frac{dw}{dx} + \frac{f(x)}{EA} = 0 \tag{A.1}$$

$$EI\frac{d^4w}{dx^4}+kEA\frac{du_0}{dx}+k^2EAw=q(x)+e\frac{df(x)}{dx} \tag{A.2}$$

where u_0 is displacement at the central point of the section along the beam axis, $k=k_{11}$, $w=w_3$, and A is the area of beam section. Considering the configuration of beam deformation, the displacement u_0 along the beam axis can be related to the displacement on the shell u

$$u_0=u+e\frac{dw}{dx} \tag{A.3}$$

Substituting Eq. (A.3) into (A.1) and (A.2) gives

$$\frac{d^2u}{dx^2}+k\frac{dw}{dx}+e\frac{d^3w}{dx^3}+\frac{f(x)}{EA}=0 \tag{A.4}$$

$$EI\frac{d^4w}{dx^4}+2ekEA\frac{d^2w}{d^2x}+kEA\frac{du}{dx}+k^2EAw=q(x)+e\frac{df(x)}{dx} \tag{A.5}$$

Eq. (A.5) can be written as

$$(EI+EA\,e^2)\frac{d^4w}{dx^4}+2ekEA\frac{d^2w}{d^2x}+k^2EAw=q(x)-EA\left[e\frac{d^3u}{d^3x}+k\frac{du}{dx}\right] \tag{A.6}$$

The characteristic equation for the differential equation (A.6) is given by

$$\beta^4+2\lambda\beta^2+\alpha^2=0 \tag{A.7}$$

where

$$\lambda=\frac{ekA}{I+e^2A},\qquad \alpha=k\sqrt{\frac{A}{I+e^2A}}$$

As $\lambda<\alpha$, the four roots of Eq. (A.7) can be found $\beta=\pm\xi\pm i\eta$, where $\xi=\sqrt{\alpha}\cos\phi$, $\eta=\sqrt{\alpha}\sin\phi$ and

$$\phi=\frac{\pi}{2}+\tan^{-1}\frac{\lambda}{\sqrt{\alpha^2-\lambda^2}}$$

The general solution of Eq. (A.6) can be written as

$$\tilde{w}(x)=e^{\xi x}(A\cos\eta x+B\sin\eta x)+e^{-\xi x}(C\cos\eta x+D\sin\eta x) \tag{A.8}$$

By use of an interpolation function, the interaction forces and moment can be approximated as

$$q(x)=\sum_{n=1}^{N}L_n(x)q^n,\qquad f(x)=\sum_{n=1}^{N}L_n(x)f^n \tag{A.9}$$

where N denotes the number of nodes on the beam and, q^n and f^n are the nodal values of the interaction forces. Shape functions $L_n(x)$ are given by

$$L_n(x)=\prod_{m=1,m\neq n}^{N}(x-x_m)\Big/\prod_{m=1,m\neq n}^{N}(x_n-x_m) \tag{A.10}$$

In general, the in-plane displacements $u(x)$ are unknown at the two ends of the beam. They are expressed as

$$u(x)=\sum_{n=1}^{N+2}L_n(x)u^n,\qquad w(x)=\sum_{n=1}^{N+2}L_n(x)w^n \tag{A.11}$$

where $x_{N+1} = x_L$ and $x_{N+2} = x_R$, and u^n are the nodal values of displacement. Substituting Eqs. (A.9) and (A.11) into Eq. (A.6) and solving the differential equation (A.6) results in

$$w(x) = \tilde{w}(x) + w^*(x) = e^{\xi x}(A\cos\eta x + B\sin\eta x) + e^{-\xi x}(C\cos\eta x + D\sin\eta x) + \sum_{k=0}^{N+1} a_k x^k \tag{A.12}$$

where $w^*(x)$ is a particular solution and coefficients a_k are determined by substituting $q(x)$ and $u(x)$ from Eqs. (A.9) and (A.11) into Eq. (A.6). Coefficients A, B, C and D are determined by applying boundary conditions at the two ends of the curved beam. The boundary conditions can be written as

$$w = w^{N+1}, \quad \frac{d^2w}{dx^2} = 0 \quad \text{for } x = x_L = 0$$

$$w = w^{N+2}, \quad \frac{d^2w}{dx^2} = 0 \quad \text{for } x = x_R = 0 \tag{A.13}$$

for the moment free ends, and

$$w = 0, \quad \frac{dw}{dx} = 0 \qquad \text{for } x = x_L = 0$$

$$w = 0, \quad \frac{dw}{dx} = 0 \qquad \text{for } x = x_R = 0 \tag{A.14}$$

for the clamped beam. Substituting $f(x)$ into Eq. (A.4) and solving this differential equation gives

$$\frac{1}{EA}\sum_{n=1}^{N} \bar{L}_n(x) f^n = k\bar{w}(x) + e\frac{dw}{dx} + u(x) + c_0 + c_1 x \tag{A.15}$$

where $\bar{L}_n(x) = \int\int L_n(x)\,dx\,dx$,

$$\bar{w}(x) = \int w(x)\,dx = \frac{e^{\xi x}}{\xi^2+\eta^2}[A(\xi\cos\eta x + \eta\sin\eta x) + B(\xi\sin\eta x - \eta\cos\eta x)] + \frac{e^{-\xi x}}{\xi^2+\eta^2}[C(-\xi\cos\eta x + \eta\sin\eta x) + D(-\xi\sin\eta x - \eta\cos\eta x)] + \sum_{k=0}^{N+1} a_k \frac{x^{k+1}}{k+1}$$

c_0 and c_1 are determined by the application of boundary conditions at the two ends of the beam

$$u = u^{N+1} \quad \text{for } x = x_L, \qquad u = u^{N+2} \quad \text{for } x = x_R \tag{A.16}$$

Eqs. (A.12) and (A.15) can be written in matrix form as

$$\mathbf{Rw} = \mathbf{Qq} + \mathbf{Pu} \tag{A.17}$$

and

$$\mathbf{Ef} = \mathbf{Q}'\mathbf{q} + \mathbf{R}'\mathbf{w} + \mathbf{P}'\mathbf{u} \tag{A.18}$$

Then the interaction forces nodal values can be expressed in terms of nodal values of deflection and displacement as

$$\mathbf{q} = \mathbf{Q}^{-1}\mathbf{Rw} - \mathbf{Q}^{-1}\mathbf{Pu} \tag{A.19}$$

and

$$\mathbf{f} = \mathbf{E}^{-1}[\mathbf{Q}'\mathbf{Q}^{-1}\mathbf{R} + \mathbf{R}']\mathbf{w} + \mathbf{E}^{-1}[\mathbf{P}' - \mathbf{Q}'\mathbf{Q}^{-1}\mathbf{P}]\mathbf{u} \tag{A.20}$$

References

Aliabadi, M.H., 1998. Plate Bending Analysis with Boundary Elements. Computational Mechanics Publications, Southampton.
Aliabadi, M.H., 2002. Applications in Solids and Structures. In: The Boundary Element Method, vol. 2. John Wiley, Chichester.
Aliabadi, M.H., Rooke, D.P., 1991. Numerical Fracture Mechanics. Computational Mechanics Publications/Kluwer Academic, Southampton/Dordrecht.
Barsoum, R.W., Loomis, R.W., Stewart, D.B., 1979. Analysis of through crack in cylindrical shells by quarter point elements. Int. J. Fract. 15 (3), 259–280.
Chinh, T.D., 1997. Calculation of shallow shell subject to influence of load local effect by the difference technique on irregular networks. Int. J. Numer. Meth. Eng. 40, 1749–1765.
Dirgantara, T., Aliabadi, M.H., 1999. A new boundary element formulation for shear deformable shells analysis. Int. J. Numer. Meth. Eng. 45, 1257–1275.
Dirgantara, T., Aliabadi, M.H., 2001. Dual boundary element formulation for fracture mechanics analysis of shear deformable shells. Int. J. Solids Struct. 38, 7769–7800.
Greif, R., Sanders, J.L., 1965. The effect of a stringer on the stress in a cracked sheet. J. Appl. Mech. 32, 59–66.
Huang, N.C., Li, Y.C., Russell, R.G., 1997a. Fracture mechanics of plates and shells applied to fail safe analysis of fuselage. Part I: theory. Theor. Appl. Fract. Mech. 27, 221–236.
Huang, N.C., Li, Y.C., Russell, R.G., 1997b. Fracture mechanics of plates and shells applied to fail safe analysis of fuselage. Part II: computational results. Theor. Appl. Fract. Mech. 27, 237–253.
Jaswon, M.A., Maiti, M., 1968. An integral equation formulation of plate bending problems. J. Eng. Math. (2), 83–93.
Mi, Y., Aliabadi, M.H., 1992. Dual boundary element method for three dimensional fracture mechanics analysis. Eng. Anal. Bound. Elem. 10, 161–171.
Portela, A., Aliabadi, M.H., Rooke, D.P., 1992. The dual boundary element method, effective implementation for crack problems. Int. J. Numer. Meth. Eng. 33, 1269–1287.
Romualdi, J.P., Frasier, J.T., Irwin, G.R., 1957. Crack extension force near a riveted stiffener. NRL report 4956.
Sanders, J.L., 1959. Effect of a stringer on the stress concentration due to a crack in a thin sheet. NASA TR R–13.
Salgado, N.K., Aliabadi, M.H., 1998. Boundary element method analysis of cracked stiffened sheets, reinforced by adhesively bonded patches. Int. J. Numer. Meth. Eng. 42 (2), 195–217.
Schijve, J., 1995. Multiple-site damage in aircraft fuselage structures. Fatigue Fract. Eng. Mater. Struct. 18 (3), 329–344.
Vander Weeën, F., 1982. Application of the boundary integral equation method to Reissner's plate model. Int. J. Numer. Meth. Eng. 18, 1–10.
Wen, P.H., Aliabadi, M.H., Young, A., 2002a. Plane stress and plate bending coupling in BEM analysis of shallow shells. Int. J. Numer. Meth. Eng. 48, 1107–1125.
Wen, P.H., Aliabadi, M.H., Young, A., 2002b. Boundary element analysis of reinforced shear deformable shells. Int. J. Numer. Meth. Eng. 54, 789–808.
Wrobel, L.C., 2002. Applications in Thermo-fluids and Acoustics. In: The Boundary Element Method, vol. 1. J. Wiley, Chichester.
Yahsi, O.S., Shahid, M.M., 1986. The effect of a stiffener on a cracked plate under bending. Int. J. Press. Vessels Pip. 23, 133–148.